THE JOURNAL OF BIOLOGICAL CHEMISTRY VOL. 282, NO. 4, pp. 2596–2605, January 26, 2007

Structural Characterization of the Active Site of the PduO-Type ATP:Co(I)rrinoid Adenosyltransferase from *Lactobacillus reuteri*[*]

Received for publication, October 10, 2006, and in revised form, November 10, 2006 Published, JBC Papers in Press, November 22, 2006, DOI 10.1074/jbc.M609557200

Martin St. Maurice[‡1,2], **Paola E. Mera**[§1,3], **María P. Taranto**[¶4], **Fernando Sesma**[¶4], **Jorge C. Escalante-Semerena**[§5], **and Ivan Rayment**[‡6]

From the Departments of [‡]*Biochemistry and* [§]*Bacteriology, University of Wisconsin, Madison, Wisconsin 53706 and the* [¶]*CERELA-CONICET, Tucumán, Argentina 4000*

The three-dimensional crystal structure of the PduO-type corrinoid adenosyltransferase from *Lactobacillus reuteri* (*Lr*PduO) has been solved to 1.68-Å resolution. The functional assignment of *Lr*PduO as a corrinoid adenosyltransferase was confirmed by *in vivo* and *in vitro* evidence. The enzyme has an apparent K_m^{ATP} of 2.2 μM and $K_m^{Cobalamin}$ of 0.13 μM and a k_{cat} of 0.025 s^{-1}. Co-crystallization of the enzyme with Mg-ATP resulted in well-defined electron density for an N-terminal loop that had been disordered in other PduO-type enzyme structures. This newly defined N-terminal loop makes up the lower portion of the enzyme active site with the other half being contributed from an adjacent subunit. These results provide the first detailed description of the enzyme active site for a PduO-type adenosyltransferase and identify a unique ATP binding motif at the protein N terminus. The molecular architecture at the active site offers valuable new insight into the role of various residues responsible for the human disease methylmalonic aciduria.

B_{12} (cobalamin, Cbl)[7] is an essential nutrient for animals, lower eukaryotes, and prokaryotes, but is synthesized exclusively by prokaryotes (1). Adenosylation of the corrinoid ring of Cbl generates coenzyme B_{12} (adenosylcobalamin, AdoCbl), an essential cofactor used by enzymes that catalyze intramolecular rearrangements (2–4), deaminations (5), dehydrations (6), reductions (7, 8), and reductive dehalogenations (9). Corrinoid adenosyltransferases play a key role in the biosynthesis of AdoCbl by covalently attaching the 5′-deoxyadenosyl moiety from ATP to the Co(I) ion of the corrin ring of Cbl (10, 11). These enzymes generate a biologically unique, labile cobalt-carbon bond that is the source of the unusual chemistry associated with the B_{12} cofactor. As such, understanding the mechanistic strategies of those enzymes involved in the formation of this carbon-metal bond is of considerable interest. In *Salmonella enterica*, three separate cob(I)alamin adenosyltransferases have been identified: CobA, PduO, and EutT. All cob(I)alamin adenosyltransferases identified to date belong to one of these three distinct families. CobA is the housekeeping enzyme of *S. enterica* and is involved in the anaerobic *de novo* synthesis of AdoCbl. The structure and function of this enzyme has been well characterized (12–16). The PduO and EutT enzymes, meanwhile, assimilate existing Cbl into AdoCbl. Both PduO and EutT are encoded within large, discreet operons of *S. enterica* where they play specialized roles in the catabolism of 1,2-propanediol or ethanolamine (17–19). Despite its specialized role in *S. enterica*, the PduO-type enzyme is the most widely distributed of these adenosyltransferases with homologues identified in species of archaeotes and prokaryotes, as well as in many eukaryotes, ranging from yeast to humans (19). In animals, PduO is the only cob(I)alamin adenosyltransferase enzyme available for the assimilation of dietary cobalamins into coenzyme B_{12}.

Humans, who lack the ability to synthesize Cbl *de novo*, produce AdoCbl from reduced Cbl through a PduO-type adenosyltransferase (19–21). Patients with malfunctions in this enzyme suffer from methylmalonic aciduria and metabolic ketoacidosis (22). Initial biochemical, functional, and structural characterization of PduO-type corrinoid adenosyltransferases has recently been reported, including a high-resolution three-dimensional crystal structure of the PduO-type enzyme from the archaeon *Thermoplasma acidophilum* (23), and two additional homologous structures deposited in the RCSB protein data bank (*Bacillus subtilis* Yvq*K*, 1RTY; and a putative PduO from *Mycobacterium tuberculosis*, 2G2D). These structures reveal that the enzyme is a trimer with each subunit composed of a five helix-bundle. Unfortunately, the absence of bound substrates in these crystal structures has precluded identification of

[*] This work was supported in part by Grants AR35186 (to I. R.) and GM40313 (to J. C. E.-S.) from the National Institutes of Health. The costs of publication of this article were defrayed in part by the payment of page charges. This article must therefore be hereby marked "*advertisement*" in accordance with 18 U.S.C. Section 1734 solely to indicate this fact.

The atomic coordinates and structure factors (code 2NT8) have been deposited in the Protein Data Bank, Research Collaboratory for Structural Bioinformatics, Rutgers University, New Brunswick, NJ (http://www.rcsb.org/).

[1] These two authors contributed equally to this work.

[2] Supported in part by a fellowship from the Natural Science and Engineering Research Council of Canada (NSERC).

[3] Supported in part by Training Grant T32 GM008505-13 (NIGMS, National Institutes of Health).

[4] Supported in part by Grants CABBIO 2004 and PICT 15016 from ANPCyT (Argentina).

[5] To whom correspondence may be addressed. E-mail: escalante@bact.wisc.edu.

[6] To whom correspondence may be addressed: Dept. of Biochemistry, 433 Babcock Dr., Madison, WI 53706. Tel.: 608-262-0437; Fax: 608-262-1319; E-mail: Ivan_Rayment@biochem.wisc.edu.

[7] The abbreviations used are: Cbl, cobalamin; *Lr*PduO, *L. reuteri* PduO; *Ta*PduO, *T. acidophilum* PduO; *Se*PduO, *S. enterica* PduO; HEPPS, 3-[4-(2-hydroxyethyl)-1-piperazinyl]propanesulfonic acid; AdoCbl, adenosylcobalamin; HOCbl, hydroxocobalamin; hATR, human adenosyltransferase; r.m.s., root mean-squared; GST, glutathione *S*-transferase; Pa, Pascal.

TABLE 1
Strains and plasmids
Unless otherwise stated, strains were constructed during the course of these studies.

	Genotype	Source or Ref.
Plasmids		
pET-15b	*bla*$^+$	Novagen
pCOBA17	pET15b *cobA*$_{Se}$$^+$ *bla*$^+$	Escalante-Semerena lab collection
pPDU19	pET28b *pduO*$_{Lr}$$^+$ *kan*$^+$	
pTEV3	pET31b H_6-tag, rTEV site at NdeI and Bpu1102I, MCS (NheI, NcoI EcoRI, XhoI, SacI, SmaI, BamHI, SacII, NotI, *Bpu*1102I) *bla*$^+$ *lacI*$^+$	Escalante-Semerena lab collection
pPDU22	pTEV3 *pduO*$_{Lr}$$^+$ *bla*$^+$	
Strains		
E. coli		
(JE3892)	BL21(λDE3) *F*$^-$ *dcm impT hsdS*(r_B^- m_B^-) *gal* λ(DE3)	New England Biolabs
S. enterica[a]		
TR6583	*metE205 ara-9 cobA*$^+$	K. Sanderson via J. Roth
JE1293	*cobA366*::Tn*10*d(*cat*$^+$)	Escalante-Semerena Laboratory Collection
JE8740	cobA366::Tn*10*d(*cat*$^+$)/pCOBA17	Escalante-Semerena Laboratory Collection
JE8741	*cobA366*::Tn*10*d(*cat*$^+$)/pPDU19	Escalante-Semerena Laboratory Collection
JE8742	*cobA366*::Tn*10*d(*cat*$^+$)/pET15b	Escalante-Semerena Laboratory Collection
L. reuteri[b]	Wild-type strain CRL1098	26

[a] Derivatives of *S. enterica* serovar Typhimurium strain LT2.
[b] CERELA stock collection, B_{12} producer.

a definitive location for the active site. Whereas both the CobA- and PduO-type adenosyltransferases catalyze the elimination of tripolyphosphate from ATP (a relatively rare mechanism among the vast families of ATP-utilizing enzymes), the CobA-type adenosyltransferases utilize an inverted P-loop motif for ATP binding and elimination of tripolyphosphate while the PduO-type enzymes apparently lack such a motif (12, 24, 25). Currently, there is no clear structural or biochemical characterization of the ATP binding site in a PduO-type enzyme.

Recently, *Lactobacillus reuteri* strain CRL1098 was discovered to make B_{12} *de novo* (26), and a gene putatively encoding a homolog of the *Se*PduO enzyme was identified among the cluster of B_{12} biosynthetic genes of this bacterium (GenBank™ accession number AY780645). In this study, we report the three-dimensional crystal structure of *L. reuteri* PduO-type corrinoid adenosyltransferase (*Lr*PduO) complexed with MgATP at 1.68-Å resolution and provide a kinetic characterization of the enzyme. Despite limited sequence identity (31%), the *Lr*PduO protein shares a common fold with the apo PduO protein from *T. acidophilum* (*Ta*PduO). Our structure model reveals the active site in a deep cleft at the subunit interface made up, in part, of the immediate N terminus of the protein. A description of the active site unveils a previously unseen ATP binding motif and provides a framework for better understanding the various mechanistic strategies employed by cob(I)-alamin adenosyltransferase enzymes. Further, this description of ATP binding allows fresh insight into the molecular basis for protein malfunction in mutations of the human corrinoid adenosyltransferase.

EXPERIMENTAL PROCEDURES

Construction of Expression Vectors—To generate an N-terminal $(His)_6$-tagged recombinant construct of PduO, the *L. reuteri pduO* gene (GenBank™ accession number AY780645) was PCR-amplified from *L. reuteri* strain CRL1098 genomic DNA isolated as described (27). The primers used for amplification were 5′-CGGGATCCGTGAAGATTTATACAAAAAATGG-3′ (forward), and 5′-GGAATTCTTAGCGGAAAACGTCTTTACTGTT-3′ (reverse). The PCR fragment was restriction-digested with BamHI and EcoRI and ligated into the pET-28b vector (EMD Biosciences, Inc.) generating the expression plasmid pPDU19 (Table 1), which expresses the recombinant PduO protein with a 35-amino acid N-terminal tag. To generate a recombinant protein with a rTEV protease-cleavable N-terminal $(His)_6$ tag, the *L. reuteri pduO* gene was PCR-amplified from plasmid pPDU19. The primers used for the amplification were 5′-AAAAAAACCATGGTGAAGATTTATACAAAAAATGGTGATAAAGGGC-3′ (forward) and 5′-TTTTTTGCGGCCGCTTAGCGGAAAAC-3′ (reverse). The PCR fragment was cut with NcoI and NotI and was ligated into vector pTEV3 (Table 1) yielding plasmid pPDU22. The pPDU22 vector directs the synthesis of a recombinant N-terminally tagged protein with the Tev protease site four residues upstream of the first amino acid of the *Lr*PduO protein. The N-terminal amino acid sequence of this construct is MSYYHHHHHHDYDIPTSENLYFQGASAPM$_1$V$_2$... where the location of the TEV protease cleavage site is underlined.

Strains, Media, and Chemicals—Bacterial strains and plasmids used in this study are listed in Table 1. Chemicals were purchased from Sigma. Lysogenic broth (LB) (28, 29) was used as rich medium to propagate bacteria nonselectively. Vogel and Bonner's no-carbon E (NCE) minimal medium (30, 31) was used to assess cobalamin biosynthesis. NCE medium was supplemented with glycerol (22 mM), $MgSO_4$ (1 mM), dicyanocobinamide ($(CN)_2$Cbi, 0.2 μM)), kanamycin (15 μg/ml), or ampicillin (25 μg/ml). Growth behavior was monitored at 650 nm using a Bio-Tek EL808 96-well plate reader. Each well contained 198 μl of fresh NCE medium that was inoculated with 2 μl of an overnight culture of the strain of interest grown in LB medium; each strain was analyzed in triplicate. Plates (Becton Dickinson) were incubated under aerobic conditions at 37 °C over a 24-h period.

LrPduO Protein Production and Purification—Plasmids were transformed into *Escherichia coli* strain BL21(λDE3) for overexpression. Strains were grown at 37 °C with shaking in 1 liter of LB medium supplemented with kanamycin (25 μg/ml). After the culture reached an optical density (OD_{650}) of 0.6–0.7, synthesis of the phage T7 RNA polymerase

TABLE 2
X-ray data collection and refinement statistics

Space group	I23
Unit-cell parameters (Å)	$a = b = c = 110.6$
Resolution range (Å)	50.00-1.68
Reflections: measured	243 527
Reflections: unique	25 595
Redundancy	9.5 (6.8)[a]
Completeness (%)	99.5 (99.5)
Average I/σ	43.1 (4.1)
R_{sym} (%)	4.6 (23.4)
R_{work} (%)	17.3 (21.5)
R_{free} (%)	20.4 (25.2)
No. protein atoms	1521
No. water molecules	141
Wilson B-value (Å^2)	22.0
Average B factors (Å^2)	
PduO	23.0
Mg-ATP	15.7
Solvent	37.4
Ramachandran (%)	
Most favored	96.9
Additionally allowed	2.5
Generously allowed	0
Disallowed	0.6[b]
r.m.s. deviations	
Bond lengths (Å)	0.011
Bond angles (°)	1.35

[a] Values in parentheses are for the highest resolution bin (1.74-1.68 Å resolution).
[b] Lys^{110} lies in an external loop region of high disorder.

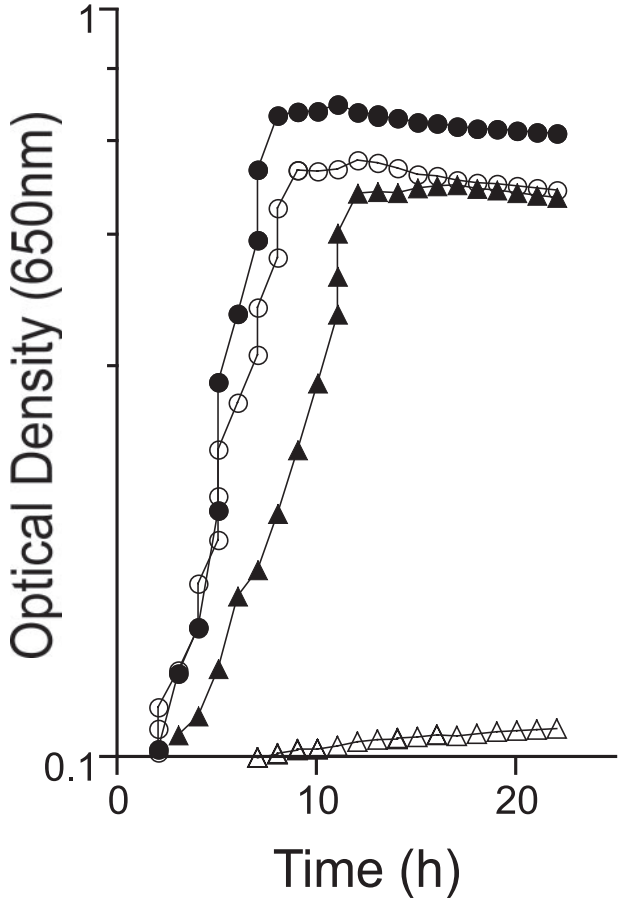

FIGURE 1. ***Lr*PduO compensates for the lack of CobA enzyme.** All strains used in these studies carried a null allele of the *metE* gene (encodes the B_{12}-independent methionine synthase) and a deletion of the *cobA* gene in their chromosome. Cells were grown in NCE minimal medium as described under "Experimental Procedures." The growth conditions used for this analysis demanded adenosylation of the precursor cobinamide prior to its conversion to AdoCbl. The following growth rates ($\Delta OD_{650}\ h^{-1}$) were calculated for each strain using the GraphPad Prism® v4 software package: *cobA*$^+$ (*closed circles*), 0.15 + 0.11; *cobA*/pET-15b (*open triangles*, empty vector control), 0.001; *cobA*/p*SecobA*$^+$ (*open circles*, positive control), 0.11 + 0.006; *cobA*/p*LrpduO*$^+$ (*closed triangles*, experiment), 0.105 + 0.009.

enzyme was induced by the addition of isopropyl-β-D-thiogalactopyranoside to a final concentration of 0.5 mM. Cells were grown for an additional 2 h at 37 °C with shaking, and harvested by centrifugation at 12,000 × *g* with a Beckman/Coulter Avanti J-25I centrifuge equipped with a JLA-16.250 rotor. The cell pellet was frozen at −80 °C until used. For protein purification, cell pellets were thawed and re-suspended in 20 ml of Tris-HCl buffer (0.1 M, pH 8.0 at 4 °C) containing the protease inhibitor phenylmethanesulfonyl fluoride (0.8 mM), imidazole (20 mM), and NaCl (0.5 M). Cells were broken using a French pressure cell (1.03×10^7 kPa); three passages ensured >99% breakage. Cell debris was separated from soluble proteins by centrifugation at 4 °C for 45 min at 45,000 × *g*. The resulting supernatant was filtered (0.45 μm; Nalgene), and proteins were resolved on a 5-ml HisTrap FF column (Amersham Biosciences). Proteins were desorbed from the column with a linear gradient of Tris-HCl buffer (0.1 M, pH 8.0 at 4 °C) containing imidazole (0.5 M) and NaCl (0.5 M); 2-ml fractions were collected. Initial estimates of protein purity were made by SDS-PAGE (32) and Coomassie Blue staining (33). Fractions containing *Lr*PduO protein of the highest purity were pooled and sequentially dialyzed at 4 °C against buffer A (Tris-HCl (0.1 M, pH 8 at 4 °C) containing NaCl (0.5 M), EDTA, 2 mM), buffer B (buffer A lacking EDTA), and buffer C (Tris-HCl (10 mM, pH 8 at 4 °C) containing NaCl (0.3 M) and Mg-ATP (3 mM)). Final protein purity was assessed with Fotodyne's FOTO/Eclipse® Electronic Documentation & Analysis System, including software packages FOTO/Analyst® PC Image v5.0 and TotalLabTM one-dimensional gel analysis v2003 from NonLinear Dynamics, Ltd. Purified *Lr*PduO protein was estimated to be >99% homogeneous and gave a yield of 40 mg from 1 liter of broth culture. This highly purified *Lr*PduO protein was flash-frozen in liquid nitrogen in 40-μl droplets and stored at −80 °C until used. *Lr*PduO protein with a TEV cleavable, N-terminal poly-His tag was overproduced from plasmid pPDU22 and initially purified as described above. Prior to dialysis, purified rTEV protease (34–36) was mixed with *Lr*PduO in a 1:50 rTEV:*Lr*PduO molar ratio, and incubated at room temperature for 3 h. The mixture was dialyzed overnight against buffer D (buffer A containing imidazole, 10 mM), followed by a 4-h dialysis at 4 °C against buffer E (Tris-HCl, 0.1 M, pH 8 at 4 °C containing NaCl, 0.5 M, and imidazole, 10 mM). The rTEV:*Lr*PduO protein mixture was loaded onto a 5-ml HisTrap FF column. The column flow-through was collected and dialyzed against Tris-HCl buffer (0.1 M, pH 8.0 at 4 °C) containing NaCl (0.5 M) and 10% (v/v) glycerol. Tag-less *Lr*PduO used for kinetic analysis was stored at −80 °C until used.

In Vitro Adenosyltransferase Activity Assay—Activity assays were performed as described (37) with the following modifications. The final volume of each reaction was 1 ml. Empty, sealed quartz cuvettes were flushed with oxygen-free N_2 for 5 min. Under a stream of O_2-free N_2, Tris-HCl (0.2 M; pH 8.0 at 37 °C),

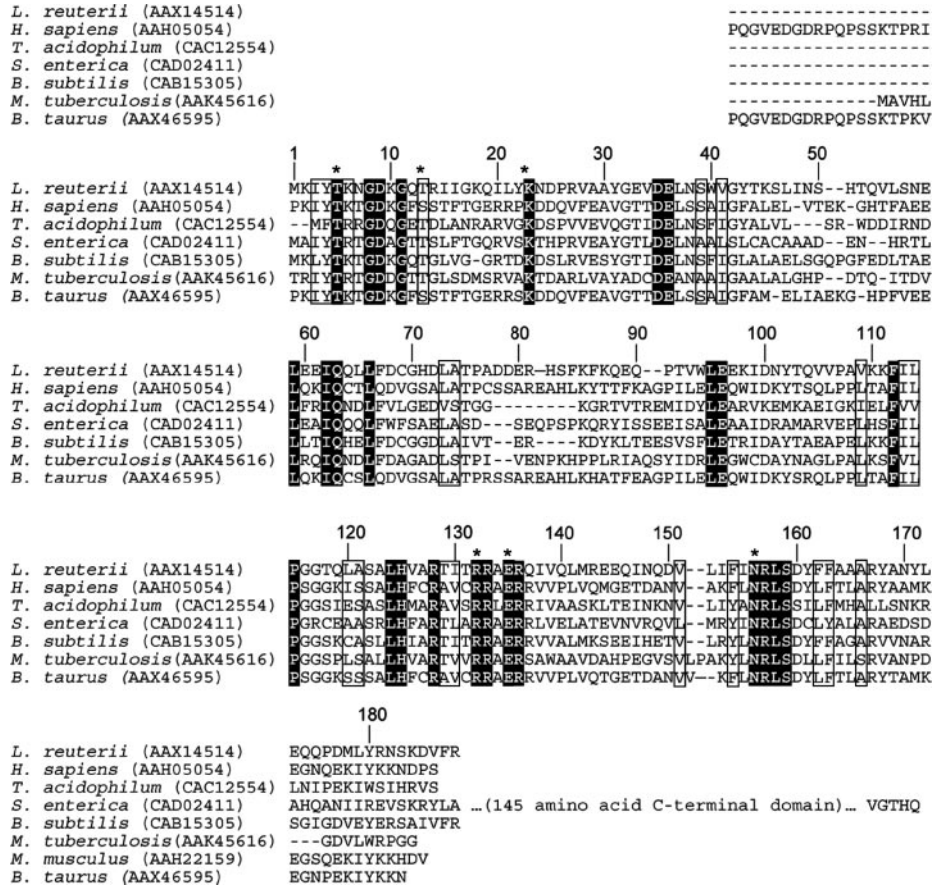

FIGURE 2. **Multiple protein sequence alignment for PduO-type adenosyltransferase enzymes.** Alignments were generated using T-Coffee (55). All aligned sequences are from confirmed structural and/or functional homologues of PduO. The sequences for both *Homo sapiens* and *B. taurus* are shown without the predicted N-terminal mitochondrion-targeting sequence and only the N-terminal domain of the *S. enterica* sequence is shown. The numbering corresponds to the sequence for the *L. reuteri* enzyme. The residues shaded in *black* are universally conserved while the *boxed* residues are strongly conserved. Residues indicated with a star are implicated in ATP binding at the active site. The GenBank™ accession numbers for each sequence are listed in parentheses.

hydroxocobalamin (HOCbl 0.1–10 μM), $MgCl_2$ (0.5 mM), ATP (1 μM-1 mM), and Ti(III)citrate (0.1 mM) were added to the cuvette in the order stated. After all additions were made, flushing was continued for 30 s. To ensure that all Co(III) was reduced to Co(I), reaction mixtures were incubated at 37 °C for 5 min. The adenosylation reaction was initiated by the addition of *Lr*PduO protein (45 nM). Adenosylcobalamin (AdoCbl) formation was monitored at 388 nm.

Crystallization and Data Collection—Crystals of the recombinant native protein, expressed with a 35-amino acid, N-terminal-$(His)_6$ tag, were grown at 20 °C in hanging drop by mixing 4 μl of 20 mg/ml protein in buffer C with 4 μl of precipitant solution composed of HEPPS (0.1 M, pH 8.5), ammonium sulfate (1.9 M, pH 8.5), $MgCl_2$ (0.1 M), and HOCbl (4 mM). The resulting solution was microseeded after 24 h, resulting in the growth of cubic-shaped, pink crystals (~300 μm^3) within 3–5 days. Crystals were transferred to a synthetic mother liquor solution containing HEPPS, (0.11 M, pH 8.5), ammonium sulfate (1.1 M, pH 8.5), ATP (2 mM), $MgCl_2$ (55 mM), NaCl (165 mM), and HOCbl (15 mM) and allowed to soak for 7 days. The coloration of the crystals darkened from pink to red over the course of the soak. The soaked crystals were incrementally transferred in five steps to a cryoprotectant solution consisting of HEPPS (0.11 M, pH 8.5), ammonium sulfate (1.2 M, pH 8.5), ATP (3 mM), $MgCl_2$ (55 mM), NaCl (0.3 M), HOCbl (15 mM), and glycerol (20% v/v) and were flash cooled in a nitrogen stream at 100 K (Oxford Cryosystems, Oxford, UK). The crystals belonged to the space group I23, with one subunit in the asymmetric unit and the unit cell parameters $a = b = c = 110.6$ Å. A dataset was collected at the SBC 19BM beamline of Advanced Photon Source in Argonne, IL. Diffraction data were integrated and scaled with the program *HKL2000* (38). Data collection are summarized in Table 2.

Structure Determination and Refinement—The structure was determined by molecular replacement with the program MOLREP (39) starting from the model for TA1434, a PduO-type cob(I)alamin adenosyltransferase from *T. acidophilum* (PDB accession identifier 1NOG, Ref. 23), for which there is 31% identity with the protein sequence of *Lr*PduO. Residues 3–181 for the *L. reuteri* enzyme were built automatically into the electron density by the program ARP/WARP (40), and the structure was refined with the program REFMAC (41). The initial structure was subject to manual verification. Multiple conformations were added with the program COOT (42). Water molecules were added to the dataset by ARP/WARP with subsequent manual verification. The final model, refined to 1.68-Å resolution, includes residues Lys^2–Asn^{182} of *Lr*PduO and the heteroatom Mg-ATP with the following 15 residues displaying multiple conformations: Gln^{19}, Lys^{45}, Ile^{48}, Val^{54}, Ser^{56}, Glu^{60}, Phe^{67}, Ser^{83}, Gln^{90}, Val^{105}, Ala^{108}, Arg^{128}, Arg^{132}, Gln^{140}, Met^{178}. Residues Met^1 and Ser^{183}-Arg^{188}, and those residues corresponding to the preceding 35 amino acids of the N-terminal tag were disordered and were not built into the model. The side chains corresponding to Arg^{14}, Glu^{60}, Lys^{85}, Gln^{104}, Lys^{110}, Lys^{111}, Gln^{146}, Arg^{181}, Asn^{182} were disordered and could not be built into the electron density map. Despite the mild red coloration of crystals grown and soaked in the presence of HOCbl, no electron density was observed in the map that could be attributed to fully occupied HOCbl. All figures of molecular structures were generated with the program PyMOL. A Ramachandran plot shows that 96.9% of the residues are in the most favored region, with one outlier that lies in a flexible loop. Refinement statistics are summarized in Table 2.

TABLE 3
Kinetic parameters for native and N-terminally tagged *Lr*PduO

Substrate varied	N-terminally tagged *Lr*PduO			Untagged *Lr*PduO (NH_2–GSASPM$_1$V$_2$K$_3$...)		
	K_m	k_{cat}	k_{cat}/K_m	K_m	k_{cat}	k_{cat}/K_m
	μM	s^{-1}	$M^{-1} s^{-1}$	μM	s^{-1}	$M^{-1} s^{-1}$
HOCb1	0.31 ± 0.05	$2.8 \pm 0.2 \times 10^{-2}$	$9.0 \pm 1.6 \times 10^{4}$	0.13 ± 0.01	$2.4 \pm 0.1 \times 10^{-2}$	$1.8 \pm 0.2 \times 10^{5}$
ATP	3.3 ± 0.8	$2.8 \pm 0.1 \times 10^{-2}$	$8.5 \pm 2.1 \times 10^{3}$	2.2 ± 0.1	$2.6 \pm 0.1 \times 10^{-2}$	$1.2 \pm 0.1 \times 10^{4}$

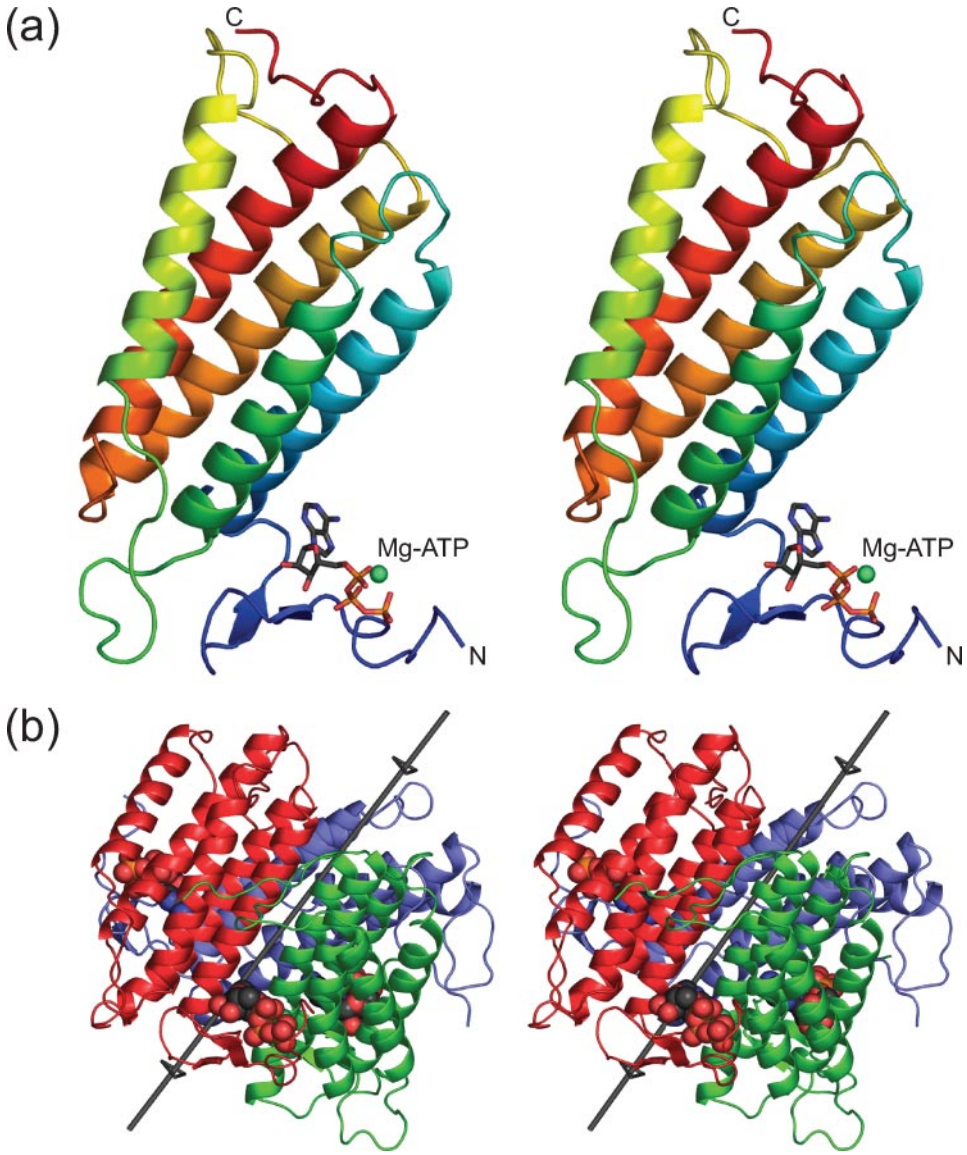

FIGURE 3. **Ribbon representations of ATP-bound LrPduO.** *a*, stereoview of a single subunit of LrPduO colored in *rainbow format*, beginning with *blue* at the N terminus and ending in *red* at the C terminus. A *stick representation* showing the position of Mg-ATP at the N-terminal binding site is also labeled. *b*, stereoview of the trimeric enzyme with the 3-fold axis of symmetry indicated. A *space-filling representation* denotes the positions of Mg-ATP.

RESULTS AND DISCUSSION

The LrPduO Protein Has ATP:Co(I)rrinoid Adenosyltransferase Enzyme Activity—Results from complementation studies involving *Lr*PduO protein are shown in Fig. 1. The growth defect of a strain of *S. enterica* lacking the housekeeping ATP:co(I)rrinoid adenosyltransferase (CobA) enzyme was corrected by the presence of a plasmid encoding the *Lr*PduO protein (Fig. 1, *closed versus open triangles*). Under the growth conditions used in this study, *S. enterica* does not express endogenous PduO, nor does it express *eutT* (44, 45). Therefore, the conditions of the above-mentioned experiments demanded that the *Lr*PduO protein adenosylate cobinamide prior to its conversion to AdoCbl (46). Hence, on the basis of these data, it is concluded that *Lr*PduO is involved in corrinoid adenosylation. Given the homology of *Lr*PduO to the N-terminal domain of *S. enterica* PduO (*Se*PduO; Fig. 2), it was hypothesized that the *Lr*PduO protein catalyzes the formation of the unique Co-C bond between the 5′-deoxyadenosyl moiety of ATP and the cobalt ion of the corrin ring.

Kinetics of the Reaction Catalyzed by LrPduO—Direct evidence that *Lr*PduO catalyzes the last step of the corrinoid adenosylation pathway (13) was obtained *in vitro*. Initial velocity kinetic determinations were performed using chemically reduced cob(I)alamin and ATP as substrates for purified *Lr*PduO protein that did or did not have an N-terminal tag. Kinetic constants were measured by holding one substrate at saturation while the other was varied (Table 3). These data confirmed that the *Lr*PduO protein has ATP:cob(I)alamin adenosyltransferase enzyme activity. The apparent K_m for ATP (K_m, 2 μM) at saturating cob(I)alamin is similar to the one reported for the human PduO-type adenosyltransferase (K_m, 6 μM) (20, 47), but is lower than that reported for the PduO enzymes from *T. acidophilum* (K_m, 110 μM) (23) and *S. enterica* (K_m, 20 μM) (48). Notably, the apparent K_m for cob(I)alamin at saturating ATP is at least 10-fold lower than any previously reported K_m value for any type of ATP:adenosyltransferase (K_m, 1–5 μM). The apparent k_{cat} for the *L. reuteri* enzyme (0.03 s^{-1}) is also lower than what has been reported for other adenosyltransferases (k_{cat} = 0.1–0.3 s^{-1}), bringing the k_{cat}/K_m values for the *L. reuteri* enzyme within the range of what has been reported for the other enzymes ($k_{cat}/K_m = 10^4$–10^5 M^{-1} s^{-1}). Our results indicate

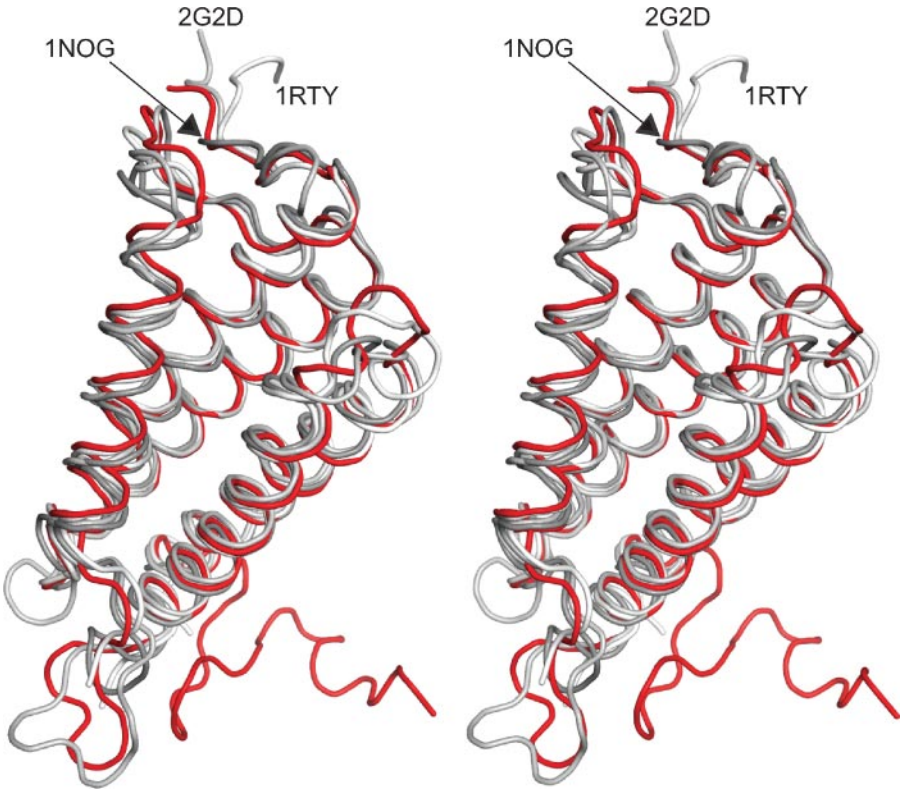

FIGURE 4. **Structural overlay of PduO-type adenosyltransferase enzymes.** Stereoview of the α-carbon backbone of *B. subtilis* YvqK (1RTY), *T. acidophilum* PduO (1NOG), and the putative PduO from *M. tuberculosis* (2G2D) aligned with the α-carbon backbone of *Lr*PduO (shown in *red*) using the program ALIGN (55). The r.m.s. deviations for alignments excluding the N-terminal 23 residues of *Lr*PduO were 0.63, 1.10, and 1.26 Å with the enzymes from *B. subtilis*, *T. acidophilum*, and *M. tuberculosis*, respectively.

that the presence of the 35-residue N-terminal tag has only a small effect on the reaction kinetics. Similar kinetic results have been reported for the N-terminal GST-tagged construct of hATR (47) and the mitochondrial targeting sequence-tagged bovine PduO (19). Based on the location of the active site at the immediate N terminus of *Lr*PduO (see the structural description below), the slightly elevated K_m values for the tagged enzyme may reflect a minor impedance of access to the active site with a concomitant reduction in the overall binding affinity.

Overall Structure and Description of the Active Site—The structure of *Lr*PduO was determined for the N-terminally tagged protein using molecular replacement, with initial phases from the crystal structure of TA1434 (PDB accession identifier 1NOG), a PduO-type ATP:cob(I)alamin adenosyltransferase from *T. acidophilum* crystallized in the absence of ligands (23), with which *Lr*PduO shares 31% sequence identity. The structure was solved for the tagged version of the enzyme, as this particular construct crystallized more readily than did the construct with the proteolytically removed tag. The final structure was refined to 1.68-Å resolution, with an R_{work} of 17.3 and an R_{free} of 20.4. As with the enzyme from *T. acidophilum*, *Lr*PduO is a trimer consisting of three independent five-helix bundles with an overall topology of 12354 (Fig. 3). The interactions between the individual helices and subunits are similar to those described for the *T. acidophilum* enzyme (23). Notably, while the immediate N terminus of all previously reported structures of PduO-type adenosyltransferases has been disordered, the structure of *Lr*PduO is unique in that it includes an additional ordered 23 amino acids at the immediate N terminus of the protein (Fig. 4). The newly defined structure of the N terminus spans residues 2–24 of the native polypeptide chain and does not include any contributions from the 35-residue N-terminal tag. Aside from this ordered N-terminal loop, no significant conformational changes accompany ATP binding, with low r.m.s. deviations (0.6–1.3 Å) for the superposition of the *Lr*PduO structure with three structures of the apoenzyme. The N terminus is well-ordered (average B-value, 23.4) and consists of a region of random coil with a helical twist followed by two antiparallel β-strands interspaced by a loop of five residues. Electron density is clearly observable for Mg-ATP within this N-terminal cleft with the positions and orientations of the phosphates and the nucleotide ring very well defined (Fig. 5*a*). The N terminus accounts for the lower half of the enzyme active site with additional residues being contributed from helix four and five of the neighboring subunit. Unlike the inverted P-loop observed for CobA (12), the ATP binding site of *Lr*PduO does not conform to any of the classic nucleotide binding structural motifs as seen in the ATP grasp or protein kinase families. The N-terminal ATP-binding loop is made up of several highly conserved residues and is clamped into position through a salt bridge between two conserved residues: Asp^9 of the N-terminal loop and Arg^{157} from helix five of the neighboring subunit. The overall backbone structure of this loop is kept rigid through a pair of backbone hydrogen bonds (Lys^6–Asp^9; Gly^8–Gly^{11}) that preserve a tight helical twist leading into the first β-strand. Both Gly^8 and Gly^{11} are conserved among homologs of *Se*PduO, further suggesting a key role in scaffolding the structure of the ATP binding loop. It appears that MgATP binding is responsible for ordering the N-terminal loop. Unfortunately, despite co-crystallization with HOCbl, only small lobes of difference electron density were observed in the vicinity of the active site, indicating low occupancy for this ligand. The binding region for HOCbl, therefore, could not be modeled with confidence. However, identification of the binding site for MgATP does place restraints on the binding site for HOCbl.

ATP Binding at the Active Site of LrPduO—Mg-ATP is bound through direct interactions with 9 residues contributed from adjacent subunits of the trimer (Fig. 5, *b* and *c*). A total of 6 residues whose side chains are directly involved in binding are conserved among PduO-type adenosyltransferase enzymes (Fig. 2). This includes the hydroxyl of Thr^{13}, which appears to be structurally conserved as either a serine or threonine. The

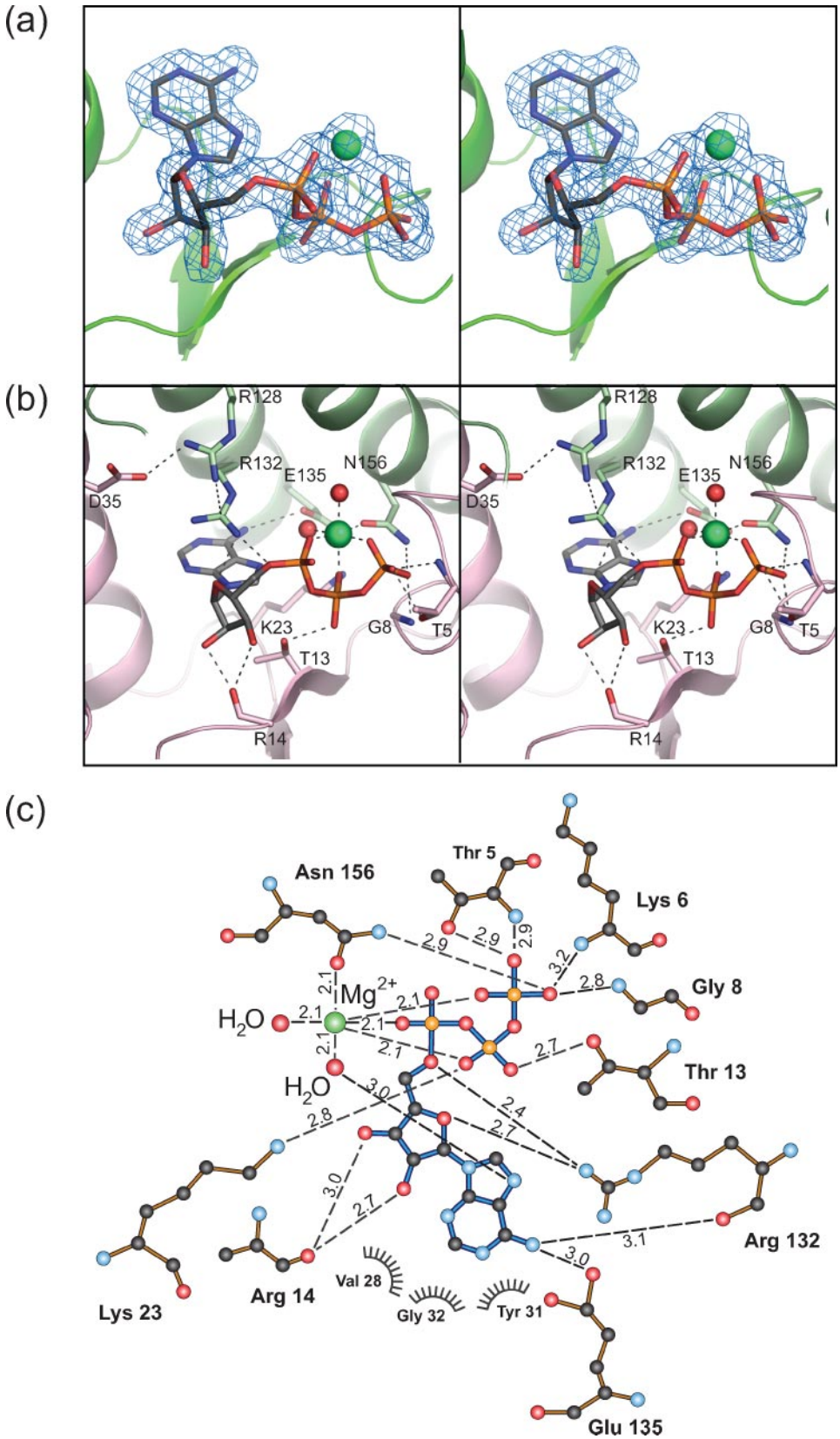

FIGURE 5. **Mg-ATP in the *Lr*PduO active site.** *a*, stereoview of the representative electron density corresponding to Mg-ATP. The F_o–F_c electron density omit map for Mg-ATP was contoured at 3.0 σ. *b*, stereoview of the active site of *Lr*PduO depicting the residues interacting with Mg-ATP. *c*, schematic representation of the interactions made by *Lr*PduO with Mg-ATP. Hydrogen bonding interactions and distances in Å are indicated. This figure was produced with the program ligplot (56). For clarity, Arg^{132} is represented in the conformation where its occupancy is the highest (~0.75) while Arg^{128} is represented in one of its two equivalent conformations.

majority of enzyme-substrate interactions are centered on the tripolyphosphate of ATP. As such, these interactions are expected to contribute significantly to ordering the N-terminal loop upon ATP binding. Several of these interactions originate from main chain amide hydrogens and carbonyls on the N-terminal loop, lending importance to the conservation of Gly^8 and Gly^{11} in maintaining the overall fold. The phosphate oxygen atoms of the enzyme-bound ATP are positioned to provide 3 coordination bonds to Mg^{2+}. In addition, two highly ordered water molecules along with the carbonyl oxygen of Asn^{156} provide the remaining coordination to the bipyramidal Mg^{2+}. Whereas many interactions with the triphosphate of ATP originate from a conserved sequence motif at the N terminus, this sequence motif appears to be unique to this class of enzymes, despite its high sequence conservation among the PduO-type adenosyltransferases (Fig. 2). A search of the protein data base using the conserved sequence Thr-(Lys/Arg)-*X*-Gly-Asp-*X*-Gly-*X*-(Thr/Ser), corresponding to residues 5–13 of the LrPduO phosphate binding domain, revealed no significant similarities with existing protein classes. Whereas the conserved amino acid sequence of PduO loosely shares features of the consensus tripolyphosphate binding sequence of the mechanistically similar adenosylmethionine synthetase and inorganic pyrophosphatase (49), a structural comparison with the active site of adenosylmethionine synthetase (50) reveals no striking similarities in the overall fold responsible for ATP binding. PduO catalyzes the elimination of tripolyphosphate from ATP (14, 48), a relatively uncommon mechanism among ATP-utilizing enzymes.

The conserved residue Arg^{132} is poised to play a critical role in stabilizing developing negative charge in the transition state and also in properly orienting the C5′-carbon of ATP for nucleophilic attack through two hydrogen bonding

TABLE 4
Relative specific activities of *Lr*PduO for alternate nucleotides

Nucleotide substrate	Relative activity
1 mM	*10 μM HOCbl*
ATP	100 ± 2%
2′-deoxy-ATP	13 ± 1%
ADP	6.6 ± 0.4%
AMP	None detected
GTP	36 ± 4%
CTP	1.4 ± 0.1%
ITP	0.8 ± 0.2%
UTP	None detected

contacts with the bridging oxygen of ribose (2.7 Å) and the bridging oxygen to the α-phosphate (2.4 Å). Whereas the precise nature of its catalytic role awaits detailed mutagenic analysis, it is noteworthy that an Arg to His mutation of the structurally equivalent residue in hATR results in a complete loss of enzyme activity (47). Interestingly, CobA has no comparable protein-ligand contacts centered around the C-5′ carbon, reinforcing the notion that the PduO- and CobA-type adenosyltransferase enzymes are mechanistically distinct despite their common overall reactions and similar efficiencies. Arg^{132}, along with the neighboring residue, Arg^{128}, displays alternate conformations in the crystal structure. In the absence of HOCbl it is difficult to assess which set of conformations is mechanistically important.

In addition to the contact between the Arg^{132} side chain and the bridging ribose, Glu^{135} and the main chain carbonyl oxygens of Arg^{132} and Arg^{14} are the only apparent bonding interactions between the protein and the adenosine base. Of these, only the side chain of Glu^{135} contacts the C-6 amine that is specific to adenine. This small number of contacts may facilitate the transfer of adenosine to cobalamin and the subsequent leaving of the first product, AdoCbl. This lack of a stringent set of binding contacts combined with a lack of tight packing around the base moiety also suggests an active site with sufficient conformational freedom to accommodate nucleotides other than ATP. While CobA type adenosyltransferases have long been known to accommodate alternate nucleotides (10, 14, 25, 51), the *Ta*PduO and *Se*PduO accept only ATP (23, 48). However, the human PduO enzyme does display moderate catalytic activity with several alternate nucleotides (19).

A survey of *Lr*PduO relative specific activities for a series of alternate nucleotides revealed specificity for a broad set of nucleotides (Table 4) with relative efficiencies similar to those described for hATR. While a detailed structural interpretation of the relative observed rates requires further kinetic analysis, it is interesting to note the low specific activity of ITP compared with ATP. The difference between these two nucleotides is limited to the identity of the functional group at the C-6 position of the purine base. Substitution at C-6 of the hydrogen bond-donating amine of ATP for the hydrogen bond-accepting carbonyl of ITP results in a 100-fold reduction in specific activity. Provided that this reduction in activity results primarily from a loss of binding affinity, the reduced specific activity with ITP may be attributed to the loss of a critical hydrogen bonding interaction with the backbone carbonyl of Arg^{132}. GTP, which also has a carbonyl at C-6, may recover a portion of this lost binding energy through a favorable potential hydrogen bonding interaction between its C-2 amine and the backbone carbonyl of Val^{28}. It is, however, more difficult to structurally interpret the reduced specific activities observed for CTP and UTP on account of the smaller relative size of the purine bases.

A subset of PduO-type enzymes is now emerging that can be defined by the ability of the enzyme to accept alternate nucleotides in place of ATP. In addition, the K_m of *Lr*PduO for ATP (3 μM) is closer to that reported for the human enzyme (7 μM) than it is to those values reported for the *Se*PduO (18 μM) or *Ta*PduO (110 μM) enzymes. Interestingly, neither humans nor lactobacilli have an identified CobA homolog, leaving the PduO-type adenosyltransferase as the only enzyme available for the conversion of Cbl to coenzyme B_{12}. In contrast, the genome of *T. acidophilum* does contain a gene encoding a putative CobA homolog (30% identical to *Se*CobA). Whether the presence of a CobA-type enzyme has an effect on the specificity and efficiency of PduO enzymes remains an open question.

The Putative Corrinoid Binding Site—The crystal structure of *Lr*PduO, like that of CobA (12), reveals ATP bound in a deep cleft at the active site. In CobA, the C-5′ carbon of ribose is positioned such that it is poised for nucleophilic attack by the reduced cobalt atom bound above. A similar scenario would be expected for the binding of cob(I)alamin in PduO. However, despite the high apparent binding affinity of cob(I)alamin for the enzyme at saturating concentrations of ATP, attempts to co-crystallize the enzyme in the presence of 2 mM HOCbl and to soak the crystals in 15 mM HOCbl did not result in any interpretable electron density for this substrate in the final structure. The crystals gained a mild red coloration when co-crystallized with HOCbl and subsequently gained a deeper red coloration upon soaking, indicating some degree of binding. Whereas HOCbl is expected to have a lower affinity than reduced cob(I)alamin, its dissociation constant for the human enzyme has been measured fluorimetrically as ~9 μM (52). It is likely that the high concentration of ammonium sulfate in the crystallization solutions significantly reduces the overall binding affinity of HOCbl for the enzyme. Attempts to co-crystallize the *Ta*PduO enzyme with cobalamin have also been unsuccessful (23). Nevertheless, it is likely that the corrinoid substrate is bound immediately adjacent to ATP in a large surface-exposed hole (Fig. 6). PduO catalyzes the direct transfer of the adenosyl moiety from ATP to reduced cobalamin, without proceeding through an enzyme-bound adenosylated intermediate (48). For such a direct transfer to take place, the corrinoid must be bound in close proximity to ATP. The hole immediately adjacent to ATP is large enough to accommodate the corrinoid but the orientation of the tetrapyrrole ring cannot be predicted because side chains lining the pocket will adopt different conformations on binding. Indeed, some lobes of electron density were interspersed throughout this hole at a signal level significantly exceeding background noise ($\sigma > 3$) and several residues lining this cavity (Asn^{19}, Phe^{67}, Ser^{83}, Ala^{108}, Arg^{128}, Arg^{132}) display alternate conformations. Furthermore, this cavity encompasses a localized area of positive electrostatic potential which may serve either to assist in binding the corrinoid substrate negatively charged phosphate moiety and/or to promote docking of

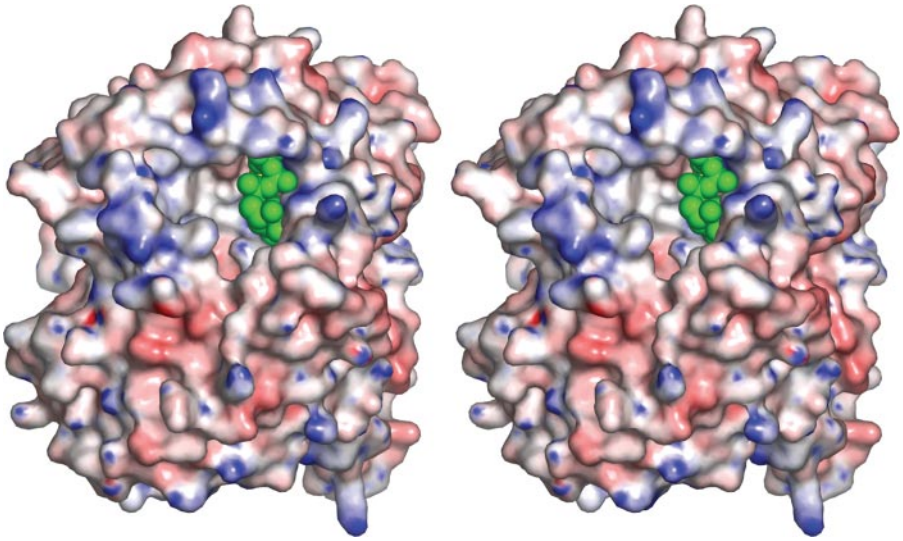

FIGURE 6. **Electrostatic surface potential stereoview for *Lr*PduO centered on the putative cobalamin binding pocket.** The electrostatic potential ranges from −20 *kT* (*red*) to +10 *kT* (*blue*). A *space-filling representation* of Mg-ATP is colored in *green*. The electrostatic potential was generated with the program APBS (57) using a protein dielectric constant of 2 and a solvent dielectric constant of 80.

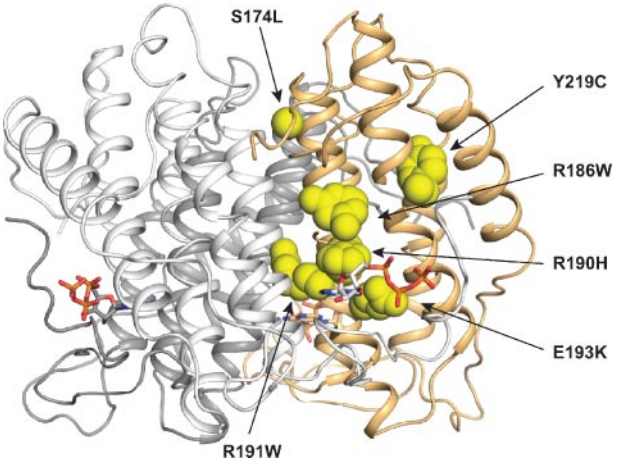

FIGURE 7. **Map of mutations identified in patients belonging to the *cblB* complementation class of methylmalonic aciduria.** The trimeric enzyme is illustrated with the human disease-related amino acid mutations (54) represented in a *yellow space-filling representation* at their equivalent position in the *Lr*PduO enzyme. For clarity, relevant amino acid mutations are shown only for the monomer highlighted in *orange*. Mutations in hATR at residues Ser^{174}, Arg^{186}, Arg^{190}, Arg^{191}, Glu^{193}, and Tyr^{219} are labeled and correspond to residues Gly^{116}, Arg^{128}, Arg^{132}, Arg^{133}, Glu^{135}, and Tyr^{161}, respectively in *Lr*PduO. The majority of mutations are clustered near the binding site for Mg-ATP. ATP is illustrated in a *stick representation*.

the putative reductase that is responsible for reducing bound cob(II)alamin to cob(I)alamin (20).

Mechanistic Insights into Methylmalonic Aciduria—The kinetic and structural characterization of the PduO-type enzyme from *L. reuteri* provides insights into the recent description of mutations in hATR responsible for methylmalonic aciduria (23, 47, 53, 54). Even though the sequence similarity between the human enzyme and *Lr*PduO enzyme is only 39%, the similar kinetic constants and nucleotide specificity provide a structural framework for understanding the biochemical consequences of the mutations. Importantly, the majority of disease-related mutations are clustered around residues contributed from helix 5 to the active site (Fig. 7). Interestingly no mutations have been identified within the phosphate binding region on the N-terminal loop.

The R186W mutation of hATR is particularly common in patients, accounting for ~30% of sequenced alleles and is associated with early onset of methylmalonic aciduria (54). Purification and characterization of the mutant enzymes R186W and R186A *in vitro* has been shown to result in a complete loss of activity (23, 47). The structurally equivalent residue of the *Lr*PduO enzyme is Arg^{128}.[8] Whereas this residue does not directly interact with ATP, it is expected to play a critical role in catalysis as evidenced by its absolute conservation among PduO-type adenosyltransferases and the complete loss of enzyme activity that results from mutations at this position. There are several possible roles for Arg^{128}. 1) Its location in the corrinoid binding pocket results in an important specific interaction with the corrin ring. Efforts to co-crystallize *Lr*PduO with various corrinoid substrates are continuing to better define the interactions between the enzyme and the corrinoid substrate. 2) It interacts directly to properly position or stabilize Arg^{132} for catalysis, or 3) it forms a critical subunit-subunit contact through a salt bridge with the absolutely conserved Asp^{35} on the adjacent subunit. On this note, it is interesting that in hATR the R186W mutation results in apparently unstable protein *in vivo* (47), suggesting that a stabilizing subunit-subunit contact is lost in these mutant enzymes.

Both R190C and R190H have been identified in patients with methylmalonic aciduria (54). This residue is structurally equivalent to Arg^{132} in the *Lr*PduO enzyme and is expected to be essential to catalysis as discussed above. It is also now clear that the E193K mutation found in patients with methylmalonic aciduria (equivalent to Glu^{135} in *Lr*PduO) will result in the loss of a specific interaction with ATP in the active site and in the loss of a critical secondary residue responsible for positioning one of two Mg^{2+}-coordinating water molecules in the active site.

The structure of *Lr*PduO presented here answers many of the questions of how nucleotides bind to this class of adenosyltransferase, but other questions remain. In particular, knowledge of how the corrinoid binds in the active site is required to establish a molecular mechanism for adenosyltransfer and the

[8] Arg^{128} has two conformations in the *Lr*PduO structure. Each conformation has independently been observed in other deposited structures of PduO. In one conformation, Arg^{128} forms an ideal salt bridge with Asp^{35} (this single conformation has also been observed in the coordinates 2G2D and 1RTY, for putative PduOs from *M. tuberculosis* and *B. subtilis*, respectively) whereas in the alternate conformation, the guanidinium functional group is shifted to position a nitrogen directly above the guanidinium group of Arg^{132}. (This equivalent position was observed in the coordinates 1NOG for the *T. acidophilum* enzyme.)

role of conserved residues. The current study establishes the foundation for these future investigations.

Acknowledgments—Use of the Structural Biology BM19 beamline Argonne National Laboratory Advanced Photon Source was supported by the United States Dept. of Energy, Office of Energy Research, under Contract No. W-31-109-ENG-38.

REFERENCES

1. Warren, M. J., Raux, E., Schubert, H. L., and Escalante-Semerena, J. C. (2002) *Nat. Prod. Rep.* **19,** 390–412
2. Halpern, J. (1985) *Science* **227,** 869–875
3. Buckel, W., Bröker, G., Bothe, H., and Pierik, A. (1999) in *Chemistry and Biochemistry of B12* (Banerjee, R., ed) pp. 757–781, John Wiley & Sons, Inc., New York
4. Banerjee, R., and Chowdhury, S. (1999) in *Chemistry and Biochemistry of B12* (Banerjee, R., ed) pp. 707–729, John Wiley & Sons, Inc., New York
5. Bandarian, V., and Reed, G. H. (1999) in *Chemistry ad Biochemistry of B12* (Banerjee, R., ed) pp. 811–833, John Wiley & Sons, Inc., New York
6. Toraya, T. (1999) in *Chemistry and Biochemistry of B12* (Banerjee, R., ed) pp. 783–809, John Wiley & Sons, Inc., New York
7. Fontecave, M. (1998) *Cell. Mol. Life Sci.* **54,** 684–695
8. Fontecave, M., and Mulliez, E. (1999) in *Chemistry and Biochemistry of B12* (Banerjee, R., ed) pp. 731–756, John Wiley & Sons, Inc., New York
9. Wohlfarth, G., and Diekert, G. (1999) in *Chemistry and Biochemistry of B12* (Banerjee, R., ed) pp. 871–893, John Wiley & Sons, Inc., New York
10. Vitols, E., Walker, G. A., and Huennekens, F. M. (1966) *J. Biol. Chem.* **241,** 1455–1461
11. Huennekens, F. M., Vitols, K. S., Fujii, K., and Jacobsen, D. W. (1982) in B_{12} (Dolphin, D., ed) Vol. 1, pp. 145–168, John Wiley & Sons, Inc., New York
12. Bauer, C. B., Fonseca, M. V., Holden, H. M., Thoden, J. B., Thompson, T. B., Escalante-Semerena, J. C., and Rayment, I. (2001) *Biochemistry* **40,** 361–374
13. Fonseca, M. V., and Escalante-Semerena, J. C. (2001) *J. Biol. Chem.* **276,** 32101–32108
14. Fonseca, M. V., Buan, N. R., Horswill, A. R., Rayment, I., and Escalante-Semerena, J. C. (2002) *J. Biol. Chem.* **277,** 33127–33131
15. Stich, T. A., Buan, N. R., Escalante-Semerena, J. C., and Brunold, T. C. (2005) *J. Am. Chem. Soc.* **127,** 8710–8719
16. Buan, N. R., and Escalante-Semerena, J. C. (2005) *J. Biol. Chem.* **280,** 40948–40956
17. Buan, N. R., Suh, S. J., and Escalante-Semerena, J. C. (2004) *J. Bacteriol.* **186,** 5708–5714
18. Buan, N. R., and Escalante-Semerena, J. C. (2006) *J. Biol. Chem.* **281,** 16971–16977
19. Leal, N. A., Park, S. D., Kima, P. E., and Bobik, T. A. (2003) *J. Biol. Chem.* **278,** 9227–9234
20. Leal, N. A., Olteanu, H., Banerjee, R., and Bobik, T. A. (2004) *J. Biol. Chem.* **279,** 47536–47542
21. Stich, T. A., Yamanishi, M., Banerjee, R., and Brunold, T. C. (2005) *J. Am. Chem. Soc.* **127,** 7660–7661
22. Ciani, F., Donati, M. A., Tulli, G., Poggi, G. M., Pasquini, E., Rosenblatt, D. S., and Zammarchi, E. (2000) *Crit. Care Med.* **28,** 2119–2121
23. Saridakis, V., Yakunin, A., Xu, X., Anandakumar, P., Pennycooke, M., Gu, J., Cheung, F., Lew, J. M., Sanishvili, R., Joachimiak, A., Arrowsmith, C. H., Christendat, D., and Edwards, A. M. (2004) *J. Biol. Chem.* **279,** 23646–23653
24. Smith, C. A., and Rayment, I. (1996) *Biophys. J.* **70,** 1590–1602
25. Buan, N. R., Rehfeld, K., and Escalante-Semerena, J. C. (2006) *J. Bacteriol.* **188,** 3543–3550
26. Taranto, M. P., Vera, J. L., Hugenholtz, J., De Valdez, G. F., and Sesma, F. (2003) *J. Bacteriol.* **185,** 5643–5647
27. Pospiech, A., and Neumann, B. (1995) *Trends Genet.* **11,** 217–218
28. Bertani, G. (1951) *J. Bacteriol.* **62,** 293–300
29. Bertani, G. (2004) *J. Bacteriol.* **186,** 595–600
30. Vogel, H. J., and Bonner, D. M. (1956) *J. Biol. Chem.* **218,** 97–106
31. Berkowitz, D., Hushon, J. M., Whitfield, H. J., Roth, J., and Ames, B. N. (1968) *J. Bacteriol.* **96,** 215–220
32. Laemmli, U. K. (1970) *Nature* **227,** 680–685
33. Sasse, J. (1991) in *Current Protocols in Molecular Biology* (Ausubel, F. A., Brent, R., Kingston, R. E., Moore, D. D., Seidman, J. G., Smith, J. A., and Struhl, K., eds) Vol. 1, pp. 10.6.1–10.6.8, Wiley Interscience, New York
34. Haspel, J., Blanco, C., Jacob, J., and Grumet, M. (2001) *BioTechniques* **30,** 60–61, 64–66
35. Kapust, R. B., and Waugh, D. S. (2000) *Protein Expr. Purif.* **19,** 312–318
36. Shih, Y. P., Wu, H. C., Hu, S. M., Wang, T. F., and Wang, A. H. (2005) *Protein Sci.* **14,** 936–941
37. Johnson, C. L., Pechonick, E., Park, S. D., Havemann, G. D., Leal, N. A., and Bobik, T. A. (2001) *J. Bacteriol.* **183,** 1577–1584
38. Otwinowski, Z., and Minor, W. (1997) *Methods Enzymol.* **276,** 307–326
39. Vagin, A., and Teplyakov, A. (1997) *J. Appl. Crystallogr.* **30,** 1022–1025
40. Perrakis, A., Harkiolaki, M., Wilson, K. S., and Lamzin, V. S. (2001) *Acta Crystallogr. D Biol. Crystallogr.* **57,** 1445–1450
41. Murshudov, G. N., Vagin, A. A., and Dodson, E. J. (1997) *Acta Crystallogr. D Biol. Crystallogr.* **53,** 240–255
42. Emsley, P., and Cowtan, K. (2004) *Acta Crystallogr. D Biol. Crystallogr.* **60,** 2126–2132
43. Deleted in proof
44. Ailion, M., Bobik, T. A., and Roth, J. R. (1993) *J. Bacteriol.* **175,** 7200–7208
45. Sheppard, D. E., and Roth, J. R. (1994) *J. Bacteriol.* **176,** 1287–1296
46. Escalante-Semerena, J. C., Suh, S. J., and Roth, J. R. (1990) *J. Bacteriol.* **172,** 273–280
47. Zhang, J., Dobson, C. M., Wu, X., Lerner-Ellis, J., Rosenblatt, D. S., and Gravel, R. A. (2006) *Mol. Genet. Metab.* **87,** 315–322
48. Johnson, C. L., Buszko, M. L., and Bobik, T. A. (2004) *J. Bacteriol.* **186,** 7881–7887
49. Reczkowski, R. S., Taylor, J. C., and Markham, G. D. (1998) *Biochemistry* **37,** 13499–13506
50. Komoto, J., Yamada, T., Takata, Y., Markham, G. D., and Takusagawa, F. (2004) *Biochemistry* **43,** 1821–1831
51. Suh, S.-J., and Escalante-Semerena, J. C. (1995) *J. Bacteriol.* **177,** 921–925
52. Yamanishi, M., Labunska, T., and Banerjee, R. (2005) *J. Am. Chem. Soc.* **127,** 526–527
53. Dobson, C. M., Wai, T., Leclerc, D., Kadir, H., Narang, M., Lerner-Ellis, J. P., Hudson, T. J., Rosenblatt, D. S., and Gravel, R. A. (2002) *Hum. Mol. Genet.* **11,** 3361–3369
54. Lerner-Ellis, J. P., Gradinger, A. B., Watkins, D., Tirone, J. C., Villeneuve, A., Dobson, C. M., Montpetit, A., Lepage, P., Gravel, R. A., and Rosenblatt, D. S. (2006) *Mol. Genet. Metab.* **87,** 219–225
55. Notredame, C., Higgins, D. G., and Heringa, J. (2000) *J. Mol. Biol.* **302,** 205–217
56. Wallace, A. C., Laskowski, R. A., and Thornton, J. M. (1995) *Protein Eng* **8,** 127–134
57. Baker, N. A., Sept, D., Joseph, S., Holst, M. J., and McCammon, J. A. (2001) *Proc. Natl. Acad. Sci. U. S. A.* **98,** 10037–10041